CCS Chemistry

RESEARCH ARTICLE

Received: Oct. 29, 2020 | Accepted: Feb. 1, 2021 | Published: Apr. 7, 2021

Competition of Lamellar Crystal and Smectic Liquid Crystal in Precise Polyethylene Derivative Bearing Mesogenic Side-Chains

Wen-Ying Chang[1], Yan-Fang Zhang[1], Jing Wang[2], Dong Shi[1], Xu-Qiang Jiang[1], Xiang-Kui Ren[3]*, Shuang Yang[1]* & Er-Qiang Chen[1]*

[1]Beijing National Laboratory for Molecular Sciences, Key Laboratory of Polymer Chemistry and Physics of Ministry of Education, Center for Soft Matter Science and Engineering, College of Chemistry and Molecular Engineering, Peking University, Beijing 100871, [2]South China Advanced Institute for Soft Matter Science, South China University of Technology, Guangzhou 510640, [3]School of Chemical Engineering and Technology, Tianjin University, Tianjin 300350

**Corresponding authors: eqchen@pku.edu.cn; shuangyang@pku.edu.cn; renxiangkui@tju.edu.cn*

Cite this: *CCS Chem.* **2022**, 4, 683–692
DOI: 10.31635/ccschem.021.202000614

For side-chain liquid-crystalline polymers (SCLCPs) bearing calamitic mesogens, nematic and typical smectic (Sm) phases are expected. Here, using a precise polyethylene derivative with the biphenyl moiety tethered on every ninth carbon (P9,b), we demonstrated that an SCLCP could form a crystal (Cr) phase in addition to an Sm phase. Two opposing interrelations of main- and side-chains determined the molecular packings. While the side-chain inclined to be perpendicular to the main-chain in the Sm phase, they paralleled and coassembled in the Cr phase with an orthorhombic structure. The Sm phase of P9,b was new in SCLCPs. Within the mesogen sublayers, the biphenyls were tilted and had a type of two-dimensional positional order, making this Sm phase ordering higher than that of smectic C. The Sm phase was metastable and kinetically grew faster below its isotropic temperature. However, it could not convert to the stable Cr phase unless it transitioned into the melting state. Fantastically, P9,b rendered the lamellar crystal in the Cr phase. The lenticular lamellae resembled that found in linear polyethylene crystallized at low undercooling. Importantly, albeit having the large anisotropic pendants situated regularly in the backbone, P9,b could follow the principle of chain-folding crystallization.

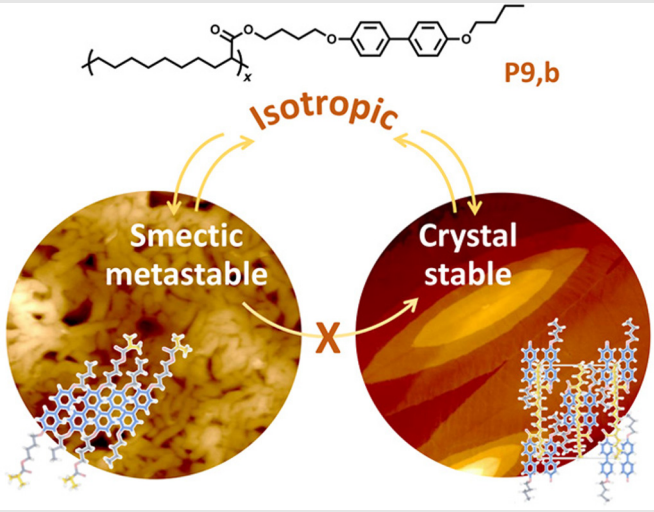

Keywords: precision polymer, side-chain liquid-crystalline polymer, polyethylene derivative, self-assembly, liquid crystal, crystallization, chain-folding lamella

DOI: 10.31635/ccschem.021.202000614
Corrected Citation: *CCS Chem.* **2022**, 4, 683–692
Previous Citation: *CCS Chem.* **2021**, 3, 763–772
Link to VoR: https://doi.org/10.31635/ccschem.021.202000614

Introduction

Typically, biological and synthetic materials are composed of different constituents that are integrated either chemically or physically, wherein the inherent competing interactions regulate the structures and dynamics, and thus, the eventual utilities.[1] When calamitic mesogens are tethered to linear-chain molecules as pendants, the resultant side-chain liquid-crystalline polymers (SCLCPs) encounter two antagonistic interactions.[2,3] Namely, the linear main-chain tends to be a three-dimensional (3D) random coil with maximal entropy; on the other hand, the mesogenic side-chains favor the anisotropic array with liquid-crystalline (LC) orders. The balance of these two aspects could lead to different LC phases, such as the nematic and smectic (Sm). Numerous SCLCPs are evidenced by having flexible spacers inserted between the calamitic mesogen and the backbone.[2-4] Thus, parallel packing of the mesogens, which are usually aromatic, could occur, accompanied by the nanosegregation between the main- and side-chains, resulting in smectic layered structures with the aliphatic main-chains confined by the mesogen sublayers.[5]

It is noteworthy that SCLCP is not simply the "backbone + mesogens." After being grafted with side-chains, the main-chain, such as linear polyethylene (PE), likely to be flexible in its archetype, would have its physical properties changed conspicuously.[6-9] Having been synthesized from vinyl monomers, the conventional SCLCPs have their mesogenic side-chains on every second carbon of the backbone. With such a high grafting density, the backbone is inevitably extended due to the remarkable steric hindrance arising from the densely arrayed side-chains.[10-12] The chain conformation is dependent mainly on the grafting density.[13-15] Advanced polymer chemistry endows the accurate placement of the branching points along the backbone; namely, one could precisely adjust the spacing between the two adjacent side-chains, and thus, the grafting density.[16-25] Enlarged side-chain spacing would enable the recovery of at least part of the backbone flexibility of SCLCPs, thereby affording more possibilities of hierarchical self-organization.[18,19,23,26-30] It has been demonstrated that, in addition to the coil conformation, when side-chain spacing is large enough, the backbones could even fold to form crystalline packing.[23,26,28,29] Recently, we found that precisely placing mesogenic side-chain on every seventh carbon rather than every second carbon along the PE backbone, the SCLCP could present a crystal structure with an order much higher than smectic LCs.[31] An important issue is the ability to control which ordered structures are probably selected in the transition pathways for the SCLCP with precise side-chain spacing and which packing mechanism would play a dominant role at the molecular level.

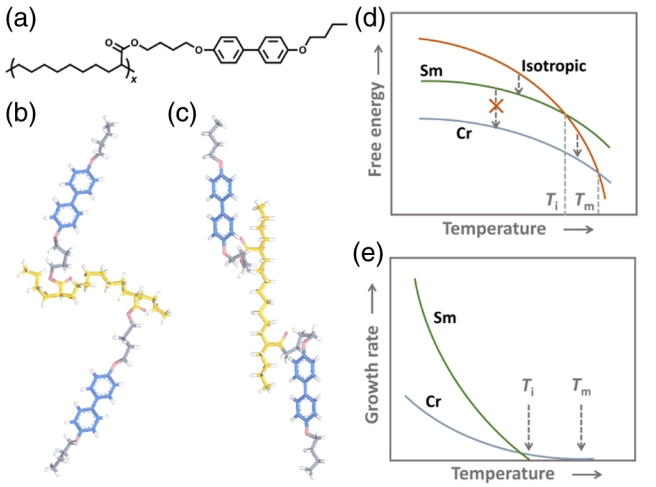

Figure 1 | *(a) Chemical structure of **P9,b**. (b and c) The interrelationship between the main- and side-chains. The side-chains could be prone to perpendicular (b) or parallel (c) to the main-chain. (d and e) Diagrams of free energy and growth rate versus temperature.* T_i *and* T_m *are the isotropic temperatures of the Sm phase and melting state of the Cr phase. The metastable Sm phase could not convert to stable Cr directly, ascribed to its growth rate being much faster than that of Cr below* T_i.

Herein, we report that the competition between LC and lamellar crystals could happen in a precise PE derivative containing a side-chain of calamitic mesogen, denoted as **P9,b** in this study (Figure 1a). The biphenyl side-chain with a butoxy tail, which had a strong tendency to form smectic packing, was situated on every ninth carbon. Two contradictory interrelations of the main- and side-chains could be envisioned for **P9,b**: the side-chain was apt to (1) perpendicular and (2) parallel to the main-chain (Figures 1b and 1c).[5,12] In **P9,b**, the roughly perpendicular conformation was associated with a new smectic LC phase (Sm), which had an order higher than the typical smectic C. In contrast, the parallel conformation led to a crystal (Cr) phase with an orthorhombic structure. Commensuration of the side-chain spacing and the mesogen length could be crucial for the synergistic array of main- and side-chains in the Cr phase, albeit metastable Sm phase could not convert to the Cr phase directly (Figure 1d) due to the thoroughly different side-chain orientations with respect to the backbone. The existence of Sm and Cr were controlled by transition kinetics (Figure 1e), and they were dependent on varying self-assembly mechanisms. Unprecedentedly, although from a chemical aspect, **P9,b** is a polymer belonging to SCLCP, it could grow lamellar crystals with lenticular shape, extending over a long period (LP; ~20 nm), and showed crystallization characteristics of chain-folding.

DOI: 10.31635/ccschem.021.202000614
Corrected Citation: *CCS Chem.* **2022**, 4, 683–692
Previous Citation: *CCS Chem.* **2021**, 3, 763–772
Link to VoR: https://doi.org/10.31635/ccschem.021.202000614

Experimental Methods

We employed acyclic diene metathesis (ADMET) polymerization, followed by backbone hydrogenation to synthesize **P9,b**.[17] The synthetic route (Supporting Information Scheme S1) details and molecular characterization are provided in the Supporting Information. Owing to the condensation polymerization mechanism of ADMET, the crude polymer had a broad range of molecular weight (MW) distribution. To eliminate the effect of low MW species on the phase transition of **P9,b**, we performed MW fractionation by preparative gel permeation chromatography. We employed gel permeation chromatography, calibrated with polystyrene standards, to measure the number-average MW of the fractionated **P9,b** as 2.1×10^4 g mol^{-1} and a polydispersity of 1.48.

Phase transition behavior of **P9,b** was investigated using differential scanning calorimetry (DSC; TA Q1000 with a mechanical refrigerator, New Castle, DE). To identify the Sm and Cr structures of **P9,b**, various diffraction experiments were conducted. One-dimensional (1D), two-dimensional (2D), and grazing-incidence (GI) X-ray diffraction (XRD) of the samples were recorded by the Ganesha system (SAXSLAB, Boston, MA) equipped with a semiconductor detector (Pilatus 300 K; DECTRIS, Baden-Daettwil, Switzerland), using Cu Kα radiation as the X-ray source (Genix3D Cu ULD; Xenocs, Grenoble, France). To obtain a well-oriented thin-film sample for the GI-XRD experiment, a drop of 20 mg/mL toluene solution of **P9,b** was spin-cast onto the substrate of a silicon wafer. Electron diffraction (ED) was performed using a JEOL JEM-F200 transmission electron microscope (TEM; Tokyo, Japan). Single crystals of **P9,b** were first grown on a carbon-coated surface of a mica sheet and then transferred to the TEM copper grid.

To inspect the crystalline lamellar morphology of **P9,b**, small-angle X-ray scattering (SAXS) was performed using the Ganesha system. We made direct observation of **P9,b** thin films spin-cast on a silicon wafer substrate using atomic force microscopy (AFM; Dimension Icon, Bruker Nano, Billerica, MA) at room temperature. PeakForce tapping mode was applied in the AFM experiments using SCANASYST-AIR probes (tip radius: ~2 nm; spring 205 constant: ~0.4 N/m; frequency: ~70 kHz). The samples' textures and their temperature variations were examined using a polarized optical microscope (POM; Nikon LV100N, Tokyo, Japan) equipped with a Linkam THMSE600 hot stage.

We calculated the relative electron-density distribution of the Sm phase based on the Fourier transform of the XRD data obtained experimentally. To simulate the molecular packing in the Cr phase, molecular mechanics simulation was performed using Materials Studio software package 8.0 (Accelrys Software Inc., San Diego, CA). A more detailed description of the experiments, calculation, and simulation could be found in the Supporting Information.

Results and Discussion

Phase transition behavior

Phase transitions of **P9,b** were investigated by DSC. Figure 2a presents the DSC cooling and subsequent heating traces recorded at various scanning rates. Upon cooling, two nearby exothermic peaks, denoted as *I* and *II*, were observed, with peak *II* being the major one. Correspondingly, two endotherms (*II′* and *I′*) could be identified during heating. The large (*II′*) peak occurred at 86 °C, with latent heat nearly identical to peak *II*. On the other hand, careful examination unveiled a broad and weak endothermic process (*I′*) ranging from 95 to 110 °C, which became more apparent as the heating rate was reduced. The phase transition of **P9,b** appeared enantiotropic; we assumed that the degree of ordering increased from *I* to *II*. However, while the onsets of *II* and *II′* were relatively close to each other, the transition *I* occurred at the temperature remarkably lower than that of *I′*, namely, undercooling, indeed existed. Usually, the enantiotropic transition of LC polymers that happens in a cooling process follows an isotropic-LC-crystal sequence, wherein the first step has little undercooling because the transition between isotropic melt and LC is close to equilibrium.[32] However, as indicated above, **P9,b** exhibited a different transition behavior. Furthermore, when the sample was heated slowly (i.e., at 2.5 °C/min), an exothermic process right after peak *II′* was sensed, as indicated by the inset in Figure 2a, which resulted in the latent heat of *I′* larger than that of *I*, suggesting recrystallization had occurred.

We inferred from the DSC results that the two transitions, *I* and *II*, would be independent and associated with two distinct self-assembly structures. To test the hypothesis, 1D XRD experiments were carried out for the **P9,b** samples with varying thermal histories at room temperature. The samples were subjected to either quenching or normal cooling from the isotropic melt state, which presented a strong and broad peak centered at q (= $4\pi\sin\theta/\lambda$) of 14.22 nm^{-1} (d = 0.44 nm) and a relatively sharp one at q of 15.75 nm^{-1} (d = 0.40 nm), respectively (Figure 2b). In the low-angle region, a set of layer diffractions were detected with the first-order one at q = 2.28 nm^{-1}, evidencing a layer period of 2.75 nm (Figure 2b). This indicated that the quenched or typically cooled **P9,b** formed the Sm phase. Conversely, a completely different diffraction profile was attained after **P9,b** was annealed above the peak temperature of *II′* (86 °C). Figure 2b shows that the 90 °C-annealed sample presented multiple diffractions in both the low- and high-angle regions, signifying the Cr phase.

The Sm and Cr phases of **P9,b** could also be evidenced using POM. Figures 2c and 2d depict the POM images

DOI: 10.31635/ccschem.021.202000614
Corrected Citation: *CCS Chem.* **2022**, 4, 683–692
Previous Citation: *CCS Chem.* **2021**, 3, 763–772
Link to VoR: https://doi.org/10.31635/ccschem.021.202000614

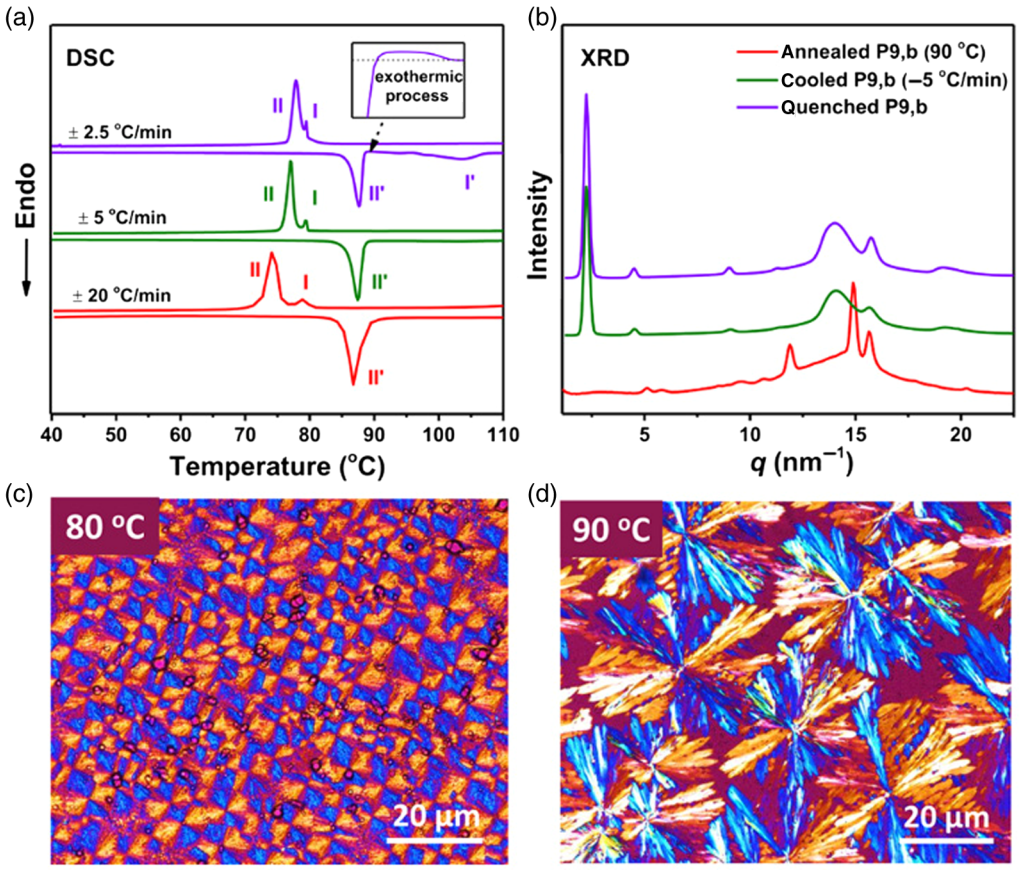

Figure 2 | *(a) DSC cooling and subsequent heating traces of **P9,b** recorded at different scan rates. The inset shows the enlarged DSC traces of the exothermic process during heating at 2.5 °C/min, wherein the dashed line indicates the baseline. (b) 1D XRD profiles recorded at room temperature of **P9,b** samples with different thermal treatments. (c and d) POM images were recorded after the samples were transferred from 120 to 80 and 90 °C, respectively. For (d), the isothermal time was 5 h.*

obtained after **P9,b**, transferred from isotropic melt to 80 and 90 °C, respectively. Fan-shaped texture appeared immediately at 80 °C (Figure 2c). In contrast, during isothermal crystallization at 90 °C, spherulite-like crystals with strong birefringence grew gradually and eventually impinged together (Figure 2d and Supporting Information Figure S1). Both Sm and Cr textures could retain upon cooling down to room temperature. Under the POM, the birefringence of Sm disappeared when the temperature exceeded 86 °C (Supporting Information Figure S2). For Cr, the birefringence started to fade away upon heating to ~100 °C and vanished eventually at 110 °C (Supporting Information Figure S3).

The experimental results indicate that the peak temperature of *II′* at 86 °C should be taken as the isotropic temperature (T_i) of the Sm phase. On the other hand, the temperature of the endotherm *I′* is, in fact, the melting temperature (T_m) of the Cr phase. Above T_i, the Cr could grow without Sm interference. However, when the melted **P9,b** was cooled below T_i, Sm developed much faster than the Cr. Because the T_i was lower than T_m, the Sm phase was metastable compared with the Cr phase (Figure 1d). Nevertheless, the Sm phase did not relax spontaneously in the Cr phase at temperatures below T_i, evidenced by the XRD and POM results obtained at room temperature. These phase transition features of **P9,b** could be delineated using free energy diagrams and growth rate versus temperature, as shown in Figures 1d and 1e, respectively. We considered that the competition of Sm and Cr phases existing in **P9,b** was controlled by the transition kinetics.

Phase structure identification

We sought to further understand the unique phase behavior of **P9,b** by performing 2D XRD experiments to elucidate the molecular packing in the Sm and Cr phases. Shearing the sample at 95 °C, followed by quenching to room temperature, produced a highly oriented film of the Sm phase. With an X-ray incident beam oriented perpendicular to the shear direction, the 2D XRD pattern (Figure 3a and Supporting Information Figure S4) showed layer diffractions on the meridian (the shear direction) and high-angle diffraction of 0.40 nm on the

DOI: 10.31635/ccschem.021.202000614
Corrected Citation: *CCS Chem.* **2022**, 4, 683–692
Previous Citation: *CCS Chem.* **2021**, 3, 763–772
Link to VoR: https://doi.org/10.31635/ccschem.021.202000614

equator. Interestingly, a large peak at 0.44 nm was tightly associated with the side-chain packing appearance in the quadrants, implying that the mesogens were tilted away from the layer normal. We presumed that the tilting manner was similar to that of the smectic I or crystal K phase identified in small molecules.[33,34] Thus, the two diffractions at 0.44 and 0.40 nm could be indexed as (110) and (020), respectively, of a monoclinic unit cell with the *c*-axis along the side-chain. In this case, the tilt was toward the longer edge of the mesogen-packing array, and the monoclinic lattice parameters of the Sm could be determined to be a = 0.61 nm, b = 0.80 nm, c = 3.18 nm, and β = 120°. Note that the value of $a\sin\beta$ equaled 0.53 nm, which was identical to the parameter a determinant for the conventional crystal E phase of biphenyl mesogen,[35] implying that there might exist a herringbone array in the Sm of **P9,b**. In this context, the Sm phase possessed an order higher than smectic C, with only short-range positional order within the layer. Nevertheless, we were aware that the diffraction at 0.44 nm was rather broad, reflecting that the correlation length along the (110) plane normal was not as long, and therefore, the **P9,b** molecules should still stay in the LC state.

We heated the oriented Sm sample stepwise and in situ recorded the 2D XRD patterns (Figures 3a and 3b and Supporting Information Figure S5). To ensure the high quality of diffraction pattern, at each selected temperature, the exposure time was 60 min. The Sm structure was retained until 85 °C (Figure 3a), afterward a ring pattern XRD showed up (Figure 3b). The ring pattern's integral intensity profile was identical to the powder XRD pattern of the Cr shown in Figure 2b. It was astonishing that during the stepwise heating, the original orientation (i.e., the layer normal parallel to the shear direction) of the Sm structure was completely lost. This outcome affirmed that the Sm and Cr of **P9,b** did not correlate with each other in terms of molecular packing. Furthermore, the thermal 2D XRD experiments confirmed that temperatures below T_i prolonged annealing, thereby hindering the Sm transfer to Cr.

Since the Cr phase grew reluctantly, the shear-induced orientation would relax during the isothermal crystallization above T_i, so it was challenging to align the Cr phase mechanically. Fortunately, we found that thin-film crystallization, which could present the 1D confinement effect,[36] could lead to flat-on lamellae of **P9,b** stacked on the solid substrate, suitable for GI-XRD measurement. The thin films were spin-cast on the silicon wafer surface, followed by isothermal melt crystallization. Figure 3c depicts the GI-XRD result obtained from the **P9,b** crystals grown at 90 °C. The diffraction geometry indicated an orthorhombic structure (Figure 3c and Supporting Information Table S1). Assuming the *c*-axis of the Cr structure was perpendicular to the substrate, the low-angle diffractions on the layer lines could be well indexed (Figure 3c). The three-strong high-angle

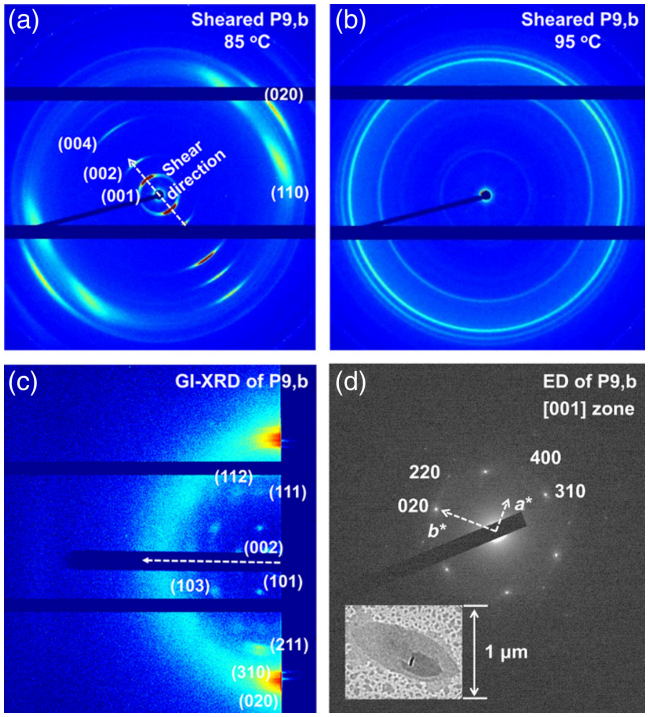

Figure 3 | *2D XRD patterns of sheared **P9,b** recorded at (a) 85 and (b) 95 °C upon heating. (c) GI-XRD pattern of **P9,b** thin film on the silicon wafer substrate after isothermal crystallization at 90 °C. The dashed arrow indicates the direction perpendicular to the substrate. (d) [001] zone ED pattern of a lamellar single crystal of **P9,b**. The inset shows the lamellar single crystal in the selected area of ED.*

diffractions observed in 1D XRD (Figures 2b and 3b) were the (211), (310), and (020) diffraction, respectively. In this case, the orthorhombic lattice of a Cr with a = 1.50 nm, b = 0.81 nm, and c = 2.19 nm was identified. The structure determination was confirmed by the selected area, ED, from a lamellar single crystal, as depicted in Figure 3d. With the electron beam perpendicular to the lamellar basal surface, the [001] zone diffraction showed apparent reciprocal lattice of (*hk*0) plane, with the parameters of a and b identical to the GI-XRD result.

Molecular packing schemes

The Sm and Cr phases of **P9,b** might have dramatically different molecular packings. As mentioned earlier, we presumed that they were associated with the various interrelations of main- and side-chains. For the Sm structure with a layer period thickness of 2.75 nm, we calculated the electron-density distribution along the smectic layer normal using the layer diffractions observed in XRD, which showed clearly a nanosegregation structure (Figure 4a and Supporting Information Figure S6). It is conceivable that the parallel packing of biphenyl

DOI: 10.31635/ccschem.021.202000614
Corrected Citation: *CCS Chem.* **2022**, 4, 683–692
Previous Citation: *CCS Chem.* **2021**, 3, 763–772
Link to VoR: https://doi.org/10.31635/ccschem.021.202000614

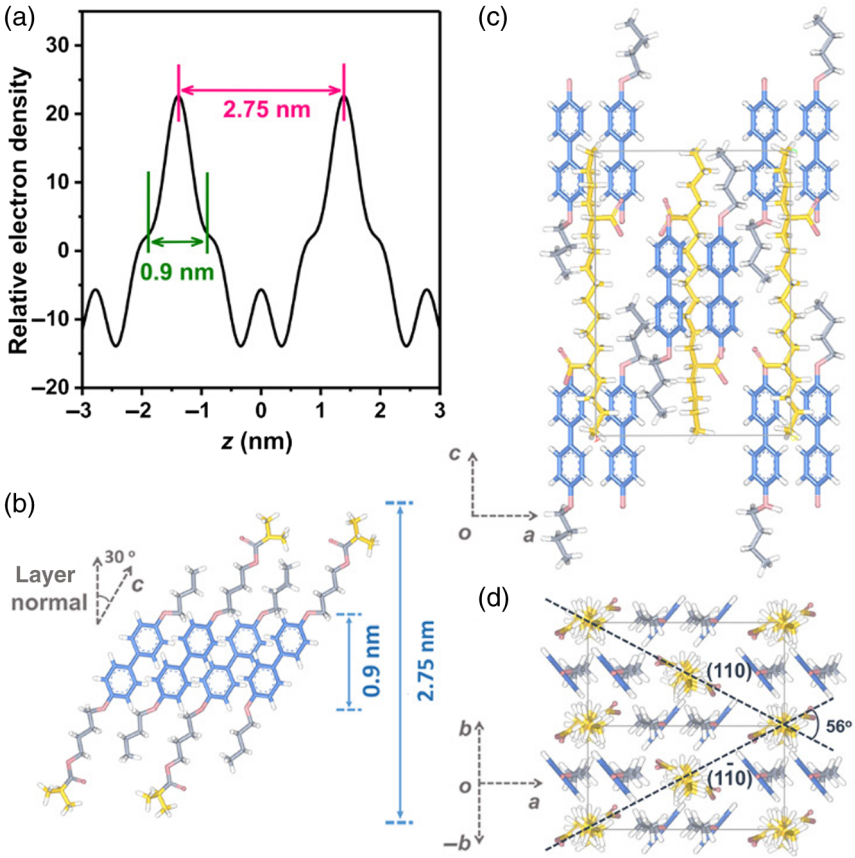

Figure 4 | *(a) 1D electron-density distribution along the smectic layer normal and (b) schematic of interdigitated and titled side-chain packing of **P9,b** in the Sm phase. To seek clarity, only the two methylene units on the backbone, which are adjacent to the side-chain, are shown in (b). (c and d) Molecular packing in the orthorhombic unit cell of the Cr phase viewed along* b- *and* c*-axes, respectively. In (d), the (110) and (1*$\bar{1}$*0) planes are indicated, showing the intersection angle of 56°. Color codes in (b–d): yellow, main-chain; red, oxygen; grey, spacer and tail; blue, biphenyl.*

moieties would result in the densest region, which could contribute to the major peak shown in the electron-density distribution. We noticed that the length of ~0.9 nm of the 30°-tilted rod-like mesogen projected on the smectic layer normal (Figure 4b), and this dimension could be found as the bottom width of the major electron density peak indicated in Figure 4a. This coincidence suggested an interdigitated packing of the mesogens in the Sm of **P9,b**, as schematically shown in Figure 4b. The lower electron density regions on both sides of the major peak should be associated with the rest of the components of **P9,b**, wherein a minor electron density peak was observed. We considered that the minor peak corresponded to the location of the main-chains, including the ester groups. In this case, it could be concluded that the nanosegregation between the main- and side-chains led to the main-chains being highly compressed in a narrow space with ~1 nm or even smaller thickness.

Notably, the **P9,b** backbone possessed eight methylene units between the two adjacent side-chains (Figure 1a). To adapt to the confined space and submit to the biphenyl packing based on π–π interaction, the methylene segment had to be curled, and the **P9,b** main-chain became an oblate random coil. In this circumstance, the main-chain and biphenyl tended to be orthogonal with each other (Figure 1b). Compared with conventional SCLCPs based on vinyl monomer, **P9,b** possessed the seven more methylene units inserted in the backbone, which would demand more space. Tilting and interdigitation of the mesogens could provide an enlarged interfacial area for each side-chain, aiding the main-chain to be accommodated without overcrowding.

Compared with the Sm phase, the chain conformation changed thoroughly when the **P9,b** molecules crystallized. We noticed that **P9,b** presented an XRD pattern with the same geometry and extinction rule as another precise side-chain LC PE (**P7**,**m**; Supporting Information Figure S7a) we reported recently, which had a side-chain on every seventh carbon and contained methoxybiphenyl rather than butyloxybiphenyl as the mesogenic moiety.[31] With the regular grafting structure, **P7**,**m** could form a crystalline phase based on coassembly of the main- and side-chains, presenting the 3D positional order.

DOI: 10.31635/ccschem.021.202000614
Corrected Citation: *CCS Chem.* **2022**, 4, 683–692
Previous Citation: *CCS Chem.* **2021**, 3, 763–772
Link to VoR: https://doi.org/10.31635/ccschem.021.202000614

According to the XRD results, **P9,b** should have the same structure. We proposed that the main- and side-chains are parallel in the Cr structure. As shown in Figure 1c, **P9,b** could adopt a parallel conformation, realized by properly rotating the ester group and the flexible spacer on the side-chains. This spatial arrangement of the main- and side-chains led to the building block of the crystal structure. It is worth mentioning that the extended length of the repeating unit on the backbone matched well with the mesogen length, both of which were ~1 nm. This commensuration could facilitate the main- and side-chains to search for a way of close packing.

Based on density measurement, we determined that the unit cell of the Cr of **P9,b** contained four repeating units. As the *c*-axis of 2.19 nm approached the extended backbone length of two repeating units (2.26 nm), two chains could be seen in the unit cell. With the aid of molecular simulation, the possible molecular packing of **P9,b** in the Cr structure with the symmetry of P*nn*2 was described (Figures 4c and 4d). The simulated XRD profile agreed quite well with the experimental data (Supporting Information Figure S7b). Interestingly, it is apparent that in the crystal lattice, two biphenyl groups could form a "pair" based on π–π interaction. Meanwhile, the PE backbone threaded through the vacancy surrounded by four biphenyl "pairs" and paralleled with the biphenyl (Figure 4d). Apparently, such a packing scheme did not maximize the π–π interaction; nevertheless, it was compensated by lowering the energy when the PE backbone assumed nearly all-*trans* conformation. Due to the ester linkages, spacers, and tail groups could have a certain degree of rotational freedom, the Cr phase had some intrinsic disorders and should be better viewed as a soft crystal.

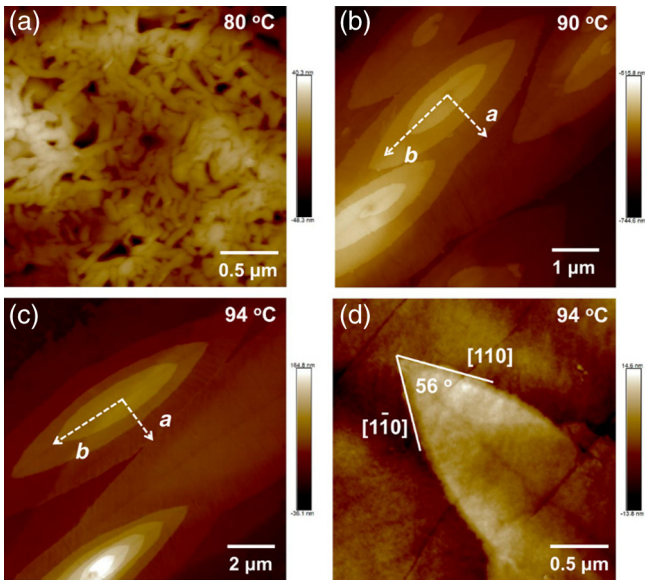

Figure 5 | *AFM images of **P9,b** thin films on the substrate of the silicon wafer. (a) The Sm phase; (b–d) The lenticular lamellar crystals. In (d), the tip of a lenticular lamella presents an angle of 56°, identical to the angle between (110) and (1$\bar{1}$0) indicated in Figure 4d.*

Lamellar crystal morphology and crystallization behavior

From a chemistry perspective, **P9,b** is a typical SCLCP. Of particular interest is what the crystal habits of **P9,b** will show up. The thin-film morphology was inspected using AFM. For comparison, we also examined the thin film of Sm phase on the silicon wafer substrate. After the spin-cast film was quenched from melting state to 80 °C, the AFM result showed that the substrate was covered by irregular entities, many of which were belt-like with a width of ~50 nm (Figure 5a). GI-XRD experiment approved that these entities were the Sm domains of which the layer normal was inclined to be approximately perpendicular to the substrate (Supporting Information Figure S8). Unexpectedly, thin-film crystallization of **P9,b** could result in a well-defined lamellar morphology. The crystallization temperature (T_c) was selected to be higher than T_i because below T_i, Sm grew so fast that it disturbed and even suppressed the crystallization of **P9,b**. AFM experiments unveiled the flat-on lamellae with lenticular shape (Figures 5b and 5c and Supporting Information Figure S9).[37–40] The lamellar stack could be induced by screw dislocation. The ED and the corresponding TEM results indicated that the short and long axes of the lenticular lamella were along the *a*- and *b*-axes of the orthorhombic lattice, respectively (Figure 3d and the inset). Compared with that grown at 90 °C, the lamellae showed a larger axial ratio of *b*/*a* when the T_c was increased to 94 °C (Figures 5b and 5c). In some areas, the (110) planes could be identified at the lamellar growth tip (Figure 5d).[40] This observation was highly reminiscent of linear PE single crystals, which were lenticular-shaped, grown from the melt state at low undercooling.[37,39,40] Therefore, despite **P9,b** having a chemical structure much more complex than linear PE, they could share some common crystallization habits.

We measured the melting behavior right after **P9,b** was crystallized at varying T_cs by DSC heating scan (Supporting Information Figure S10). Figure 6a depicts the DSC results of the samples subjected to prolonged isothermal time. Double melting was detected for the low T_cs. The small second melting should be mainly due to the occurrence of crystal perfection during heating, which became smaller with increasing T_c and disappeared when the T_c exceeded 92 °C. Long-term isothermal crystallization at T_cs of 88 ~92 °C led to the heat of fusion (ΔH_m) of 17.58 ± 0.02 kJ mol^{-1}. Assuming that this ΔH_m value was reached by complete crystallization, we estimated that the relative crystallinities, based on the ΔH_ms, were measured after the sample was isothermally

DOI: 10.31635/ccschem.021.202000614
Corrected Citation: *CCS Chem.* **2022**, 4, 683–692
Previous Citation: *CCS Chem.* **2021**, 3, 763–772
Link to VoR: https://doi.org/10.31635/ccschem.021.202000614

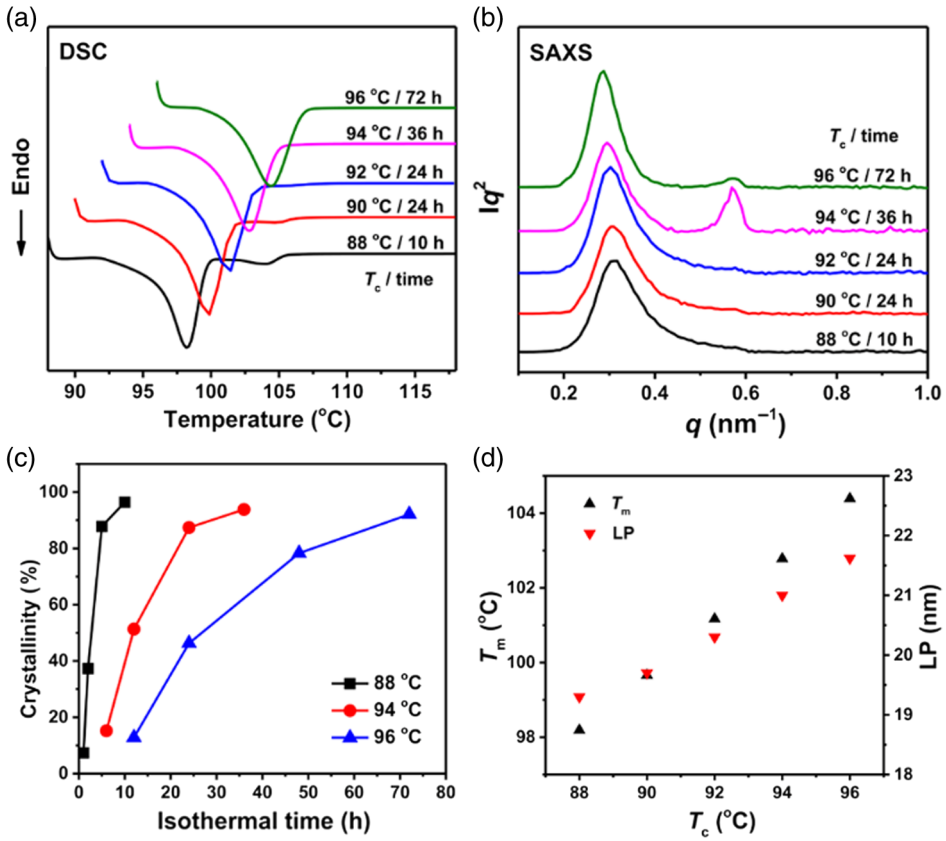

Figure 6 | *(a) DSC heating traces and (b) SAXS profiles of **P9,b** after crystallization at various* T_c*s for long isothermal times. (c) Relative crystallinity as a function of the isothermal crystallization time. (d)* T_m *and long period (LP) of **P9,b** lamellae as functions of* T_c.

crystallized at varying times. A plot of relative crystallinity as a function of time (Figure 6c) described that the crystal growth rate reduced with increasing T_c. While the formation of the Sm phase occurred in seconds, at T_c = 88 °C, just 2 °C higher than T_i, sufficient crystallization temperature of **P9,b** of 10 or more hours was required. The remarkably slow kinetics reflected the difficulty of the coassembly of main- and side-chains. Intuitively, when the flexible aliphatic parts and the anisotropic aromatic parts aligned parallel and fit into the crystal lattice, the correct conformation could only be attained after many attempts. In this case, a higher nucleation barrier existed.

We performed SAXS experiments on the isothermally crystallized samples at room temperature (Figure 6b). The lamellar LPs measured by SAXS (Figure 6d) were close to that observed in the AFM experiments (Supporting Information Figure S11). The higher the T_c, the more perfect the lamellar stacking became, evidenced by a narrow scattering peak and distinctive second-order scattering (Figure 6b). For the polymers reported with precisely placed pendant groups, the lamellar periods were usually nearly identical to the extended length of the repeating unit, which was commonly a few nanometers.[26,29] The lamellae of **P9,b** exhibited a much longer LP that could surpass 20 nm; that is, the LP of **P9,b** lamellae is almost 20 times that of the extended, repeating unit length. This suggested that the **P9,b** lamellar crystal could be formed by parallel packing of the chain stems. For **P9,b**, the elevating T_c led to the increment of LP and T_m (Figure 6d), which was the same as that found in conventional semicrystalline polymers. We assumed that if the Hoffman–Weeks plot applied to **P9,b**,[41] the linear line of T_m versus T_c would lead to an equilibrium of T_m equal to 131.5 °C. Besides, all experimental outcomes suggested that crystallization of **P9,b** should follow the principle of chain-folding.[41,42] Thus, from the XRD results, it was estimated that sufficient crystallization of **P9,b** could lead the crystallinity to reach ~60% (Supporting Information Figure S12 and Table S2). Considering the lenticular lamellae were well developed, the noncrystalline part should be associated mainly with the chain folds. The detail of the fold surface is unclear at this stage and is under investigation in our lab.

Conclusion

We have demonstrated that **P9,b**, a precise PE derivative with butyloxybiphenyl side-chains on every ninth carbon,

DOI: 10.31635/ccschem.021.202000614
Corrected Citation: *CCS Chem.* **2022**, 4, 683–692
Previous Citation: *CCS Chem.* **2021**, 3, 763–772
Link to VoR: https://doi.org/10.31635/ccschem.021.202000614

could form either an Sm or Cr phase, depending on the transition kinetics. In the Sm, the side-chains of **P9,b** were tilted, with the molecular packing order higher than that of smectic C. On the contrary, like that found in conventional SCLCPs, Sm formation was driven by the anisotropic interaction of biphenyls coupled with nano-segregation of main- and side-chains. At a temperature lower than T_i, this process took place relatively fast. The Sm phase was metastable; however, it was not the pre-order of the stable phase of Cr. This was attributable to the interrelationship between main- and side-chains in the Sm phase, which was mostly perpendicular; thus, it could not switch to the parallel one in the Cr phase unless it had gone through the isotropic state.[43] The synergistically parallel array of main- and side-chains in the Cr structure relied primarily on matching side-chain spacing and the mesogen length. We presumed that adjusting the chain from the coil to the correct parallel conformation needed time, which slowed down the nucleation and crystal growth. Intriguingly, the **P9,b** crystal was a lenticular-shaped lamella, resulting from chain-folding crystallization. Why and how the PE derivatives bearing bulky and anisotropic pendants could fold and self-assemble further into lamellar crystals are unknown at this moment. Furthermore, it is interesting to ask whether other precise side-chain LC polymers with different side-chain spacings could exhibit the crystallization behavior similar to **P9,b**. Answering these challenging questions would require an in-depth investigation to widen our understanding of polymer crystallization with characteristic chain-folding capabilities. We further envision that this unique polymer crystal type could be fabricated into advanced materials, particularly when more light- or electric-responsive mesogens are employed.

Supporting Information

Supporting Information is available and includes detailed synthesis and molecular characterization, and additional experimental data of phase transitions, structures, and morphologies.

Conflict of Interest

There is no conflict of interest to report.

Acknowledgments

The authors thank Prof. S. Z. D. Cheng for his valuable discussions. The work was supported by the National Natural Science Foundation of China (grant nos. 21634001, 21875157, and 51921002) and the National Key R&D Program of China (no. 2018YFB0703703). The TEM facility is made available by Guangdong Provincial Key Laboratory of Functional and Intelligent Hybrid Materials and Devices (nos. 2019B121203003 and 2016ZT06C322).

References

1. Muthukumar, M.; Ober, C. K.; Thomas, E. L. Competing Interactions and Levels of Ordering in Self-Organizing Polymeric Materials. *Science* **1997**, *277*, 1225–1232.
2. McArdle, C. B. *Side Chain Liquid Crystalline Polymers*; Blackie and Sons Ltd.: Glasgow, UK, **1989**.
3. Donald, A. M.; Windle, A. H.; Hanna, S. *Liquid Crystalline Polymers*; Cambridge University: Cambridge, **2006**.
4. Finkelmann, H.; Ringsdorf, H.; Wendorff, J. H. Model Considerations and Examples of Enantiotropic Liquid Crystalline Polymers. *Makromol. Chem.* **1978**, *179*, 273–276.
5. Davidson, P. X-ray Diffraction by Liquid Crystalline Side-Chain Polymers. *Prog. Polym. Sci.* **1996**, *21*, 893–950.
6. Wei, Y.; Graf, R.; Sworen, J. C.; Cheng, C.-Y.; Bowers, C. R.; Wagener, K. B.; Spiess, H. W. Local and Collective Motions in Precise Polyolefins with Alkyl Branches: A Combination of ^{2}H and ^{13}C Solid-State NMR Spectroscopy. *Angew. Chem. Int. Ed.* **2009**, *48*, 4617–4620.
7. Das, J.; Yoshida, M.; Fresco, Z. M.; Choi, T.-L.; Frechet, J. M. J.; Chakraborty, A. K. A Dendronized Polymer Is a Single-Molecule Glass. *J. Phys. Chem. B* **2005**, *109*, 6535–6543.
8. Rosen, B. M.; Wilson, C. J.; Wilson, D. A.; Peterca, M.; Imam, M. R.; Percec, V. Dendron-Mediated Self-Assembly, Disassembly, and Self-Organization of Complex Systems. *Chem. Rev.* **2009**, *109*, 6275–6540.
9. Paturej, J.; Sheiko, S. S.; Panyukov, S.; Rubinstein, M. Molecular Structure of Bottlebrush Polymers in Melts. *Sci. Adv.* **2016**, *2*, e1601478.
10. Duran, R.; Guillon, D.; Gramain, P.; Skoulios, A. Novel Mesomorphic Order in Side-Chain Polymers-Palisades of Ribbons Stacked in One Dimension. *Makromol. Chem., Rapid Commun.* **1987**, *8*, 321–324.
11. Kannan, R. M.; Kornfield, J. A.; Schwenk, N.; Boeffel, C. Rheology of Side-Group Liquid-Crystalline Polymers: Effect of Isotropic-Nematic Transition and Evidence of Flow Alignment. *Macromolecules* **1993**, *26*, 2050–2056.
12. Wang, R.; Wang, Z.-G. Theory of Side-Chain Liquid Crystal Polymers: Bulk Behavior and Chain Conformation. *Macromolecules* **2010**, *43*, 10096–10106.
13. Kikuchi, M.; Nakano, R.; Jinbo, Y.; Saito, Y.; Ohno, S.; Togashi, D.; Enomoto, K.; Narumi, A.; Haba, O.; Kawaguchi, S. Graft Density Dependence of Main Chain Stiffness in Molecular Rod Brushes. *Macromolecules* **2015**, *48*, 5878–5886.
14. Morozova, S.; Lodge, T. P. Conformation of Methylcellulose as a Function of Poly(ethylene glycol) Graft Density. *ACS Macro Lett.* **2017**, *6*, 1274–1279.
15. Lin, T.-P.; Chang, A. B.; Luo, S.-X.; Chen, H.-Y.; Lee, B.; Grubbs, R. H. Effects of Grafting Density on Block Polymer Self-Assembly: From Linear to Bottlebrush. *ACS Nano* **2017**, *11*, 11632–11641.
16. Wagener, K. B.; Boncella, J. M.; Nel, J. G. Acyclic Diene Metathesis (ADMET) Polymerization. *Macromolecules* **1991**, *24*, 2649–2657.

DOI: 10.31635/ccschem.021.202000614
Corrected Citation: *CCS Chem.* **2022**, 4, 683–692
Previous Citation: *CCS Chem.* **2021**, 3, 763–772
Link to VoR: https://doi.org/10.31635/ccschem.021.202000614

17. Inci, B.; Wagener, K. B. Decreasing the Alkyl Branch Frequency in Precision Polyethylene: Pushing the Limits toward Longer Run Lengths. *J. Am. Chem. Soc.* **2011**, *133*, 11872–11875.
18. Li, H.; Rojas, G.; Wagener, K. B. Precision Long-Chain Branched Polyethylene via Acyclic Diene Metathesis Polymerization. *ACS Macro Lett.* **2015**, *4*, 1225–1228.
19. Middleton, L. R.; Szewczyk, S.; Azoulay, J.; Murtagh, D.; Rojas, G.; Wagener, K. B.; Cordaro, J.; Winey, K. I. Hierarchical Acrylic Acid Aggregate Morphologies Produce Strain-Hardening in Precise Polyethylene-Based Copolymers. *Macromolecules* **2015**, *48*, 3713–3724.
20. da Silva, L. C.; Rojas, G.; Schulz, M. D.; Wagener, K. B. Acyclic Diene Metathesis Polymerization: History, Methods and Applications. *Prog. Polym. Sci.* **2017**, *69*, 79–107.
21. Li, H.; Rojas, G.; Wagener, K. B. Long-Chain Branched Random Polyethylene via Acyclic Diene Metathesis (ADMET) Copolymerization. *J. Polym. Sci. A Polym. Chem.* **2018**, *56*, 1705–1710.
22. Reck, B.; Ringsdorf, H. Synthesis and Phase Behaviour of Liquid-Crystalline Side Group Polyesters. *Liq. Cryst.* **1990**, *8*, 247–262.
23. Mandal, J.; Prasad, S. K.; Rao, D. S. S.; Ramakrishnan, S. Periodically Clickable Polyesters: Study of Intrachain Self-Segregation Induced Folding, Crystallization, and Mesophase Formation. *J. Am. Chem. Soc.* **2014**, *136*, 2538–2545.
24. Chanda, S.; Ramakrishnan, S. Controlling Interlamellar Spacing in Periodically Grafted Amphiphilic Copolymers. *Macromolecules* **2016**, *49*, 3254–3263.
25. Busch, H.; Majumder, S.; Reiter, G.; Mecking, S. Semicrystalline Long-Chain Polyphosphoesters from Polyesterification. *Macromolecules* **2017**, *50*, 2706–2713.
26. Buitrago, C. F.; Jenkins, J. E.; Opper, K. L.; Aitken, B. S.; Wagener, K. B.; Alam, T. M.; Winey, K. I. Room Temperature Morphologies of Precise Acid- and Ion Containing Polyethylenes. *Macromolecules* **2013**, *46*, 9003–9012.
27. Lv, J. A.; Liu, Y.; Wei, J.; Chen, E.; Qin, L.; Yu, Y. Photocontrol of Fluid Slugs in Liquid Crystal Polymer Microactuators. *Nature* **2016**, *537*, 179–184.
28. Majumder, S.; Busch, H.; Poudel, P.; Mecking, S.; Reiter, G. Growth Kinetics of Stacks of Lamellar Polymer Crystals. *Macromolecules* **2018**, *51*, 8738–8745.
29. Trigg, E. B.; Gaines, T. W.; Marechal, M.; Moed, D. E.; Rannou, P.; Wagener, K. B.; Stevens, M. J.; Winey, K. I. Self-Assembled Highly Ordered Acid Layers in Precisely Sulfonated Polyethylene Produce Efficient Proton Transport. *Nat. Mater.* **2018**, *17*, 725–731.
30. Sarkar, R.; Gowd, E. B.; Ramakrishnan, S. Precise Control of Grafting Density in Periodically Grafted Amphiphilic Copolymers: An Alternate Strategy to Fine-Tune the Lamellar Spacing in the Sub-10 nm Regime. *Polym. Chem.* **2020**, *11*, 4143–4154.
31. Chang, W.-Y.; Shi, D.; Jiang, X.-Q.; Jiang, J.-D.; Zhao, Y.; Ren, X.-K.; Yang, S.; Chen, E.-Q. Precise Polyethylene Derivatives Bearing Mesogenic Side-Chains: Delicate Self-Assembly Depending on Graft Density. *Polym. Chem.* **2020**, *11*, 1454–1461.
32. Cheng, S. Z. D. *Phase Transitions in Polymers: The Role of Metastable States*; Elsevier Science: Holand, **2008**.
33. Gane, P. A. C.; Leadbetter, A. J.; Wrighton, P. G. Structure and Correlations in Smectic B, F and I Phases. *Mol. Cryst. Liq. Cryst.* **1981**, *66*, 247–266.
34. Demus, D.; Goodby, J.; Gray, G. W.; Spiess, H.-W.; Vill, V. *Handbook of Liquid Crystals*; Wiley-VCH: Weinheim, **1998**.
35. Xie, H.-L.; Jie, C.-K.; Yu, Z.-Q.; Liu, X.-B.; Zhang, H.-L.; Shen, Z.; Chen, E.-Q.; Zhou, Q.-F. Hierarchical Supramolecular Ordering with Biaxial Orientation of a Combined Main-Chain Side-Chain Liquid-Crystalline Polymer Obtained from Radical Polymerization of 2-Vinylterephthalate. *J. Am. Chem. Soc.* **2010**, *132*, 8071–8080.
36. Liu, Y.-X.; Chen, E.-Q. Polymer Crystallization of Ultrathin Films on Solid Substrates. *Coordin. Chem. Rev.* **2010**, *254*, 1011–1037.
37. Bassett, D. C.; Olley, R. H.; Raheil, I. A. M. A. On Isolated Lamellae of Melt-Crystallized Polyethylene. *Polymer* **1988**, *29*, 1539–1543.
38. Toda, A. Rounded Lateral Habits of Polyethylene Single Crystals. *Polymer* **1991**, *32*, 771–780.
39. Toda, A.; Keller, A. Growth of Polyethylene Single Crystals from the Melt: Morphology. *Coll. Polym. Sci.* **1993**, *271*, 328–342.
40. Toda, A. Growth Mode and Curved Lateral Habits of Polyethylene Single Crystals. *Faraday Discuss.* **1993**, *95*, 129–143.
41. Hoffman, J. D. Kinetics of Crystallization Chain Folding in Polyethylene Revisited: Theory and Experiment from the Melt and Fractions. *Polymer* **1997**, *38*, 3151–3212.
42. Armitstead, K.; Goldbeck-Wood, G.; Keller, A. Polymer Crystallization Theories. *Adv. Polym. Sci.* **1992**, *100*, 221–312.
43. Muthukumar, M. Topological Dereliction in Polymers *Comput. Mater. Sci.* **1995**, *4*, 270–372.

DOI: 10.31635/ccschem.021.202000614
Corrected Citation: *CCS Chem.* **2022**, 4, 683–692
Previous Citation: *CCS Chem.* **2021**, 3, 763–772
Link to VoR: https://doi.org/10.31635/ccschem.021.202000614